Calculation of Nonequilibrium Hypersonic Turbulent Boundary Layers and Comparisons with Experimental Data

DENNIS M. BUSHNELL* AND IVAN E. BECKWITH†
NASA Langley Research Center, Hampton, Va.

The compressible turbulent boundary-layer equations are solved by a finite-difference procedure. The Reynolds stress is modeled by an eddy viscosity function where the mixing length is assumed to depend on the distance from the wall and the boundary-layer thickness except in the near wall region where Van Driest's exponential damping function is used. For applications to wall blowing cases, comparisons with data show that the damping factor should be taken as a function of the blowing rate. Nonequilibrium effects could be approximately accounted for by assuming that the mixing length in the midregion of the boundary layer is a function of a velocity profile shape factor. The nearly quadratic relation between total temperature and velocity observed in wall boundary layers of hypersonic nozzles could be obtained in the calculations only by using values for the total turbulent Prandtl number of 1.5 or more. Tentative models for the fluctuating density terms were used in some of the calculations. The results indicated that these terms may have large effects on low-density hypersonic boundary layers.

Nomenclature

A = $A^*\mu/\rho(\tau/\rho)^{1/2}$
A^* = function of blowing rate parameter $2B/C_f$ (see Fig. 1)
a = speed of sound
B = dimensionless blowing rate, $(\rho v)_w/(\rho u)_e$
C_f = skin-friction coefficient, $\tau_w/\frac{1}{2}\rho_e u_e^2$
C_p = specific heat at constant pressure
F = velocity profile, $\bar{u}/u_e$
f = mixing length function, Eq. (6); present function: $f_n = 0.4\, y/\delta$; $f_f = (l/\delta)_f$ (Fig. 2)
H = total enthalpy, $h + (u^2 + v^2 + w^2)/2$
H^* = form factor, δ^*/θ
H_i^* = incompressible form factor, δ_i^*/θ_i
l = mixing length, defined in Eq. (5)
M = Mach number
n = exponent in $\bar{\theta}$, F relation, Eq. (8)
$\bar{n}$ = adjustable constant in transformed η coordinate
Pr = molecular Prandtl number
Pr_T = total turbulent Prandtl number, $[\langle(\rho v)'u'\rangle/\langle(\rho v)'H'\rangle](\partial\bar{H}/\partial y)/(\partial\bar{u}/\partial y)$
Pr_t = static turbulent Prandtl number, $[\langle(\rho v)'u'\rangle/\langle(\rho v)'h'\rangle](\partial\bar{h}/\partial y)/(\partial\bar{u}/\partial y)$
p = pressure
Re_θ = Reynolds number based on momentum thickness, $\rho_e u_e \theta/\mu_e$
r = radius from axis of symmetry to surface
St = Stanton number, $[(\mu/Pr)\partial\bar{h}/\partial y]_w/(H_{aw} - H_w)\rho_e u_e$
T = temperature
u,v,w = velocity components in x, y, and z directions, respectively
u_τ = $(\tau/\rho)^{1/2}$
$\bar{v}$ = $\bar{v} + \langle\rho' v'\rangle/\bar{\rho} \approx \bar{v} - l^2(\partial\bar{\rho}/\partial y)|\partial\bar{u}/\partial y|/\bar{\rho}$
x,y,z = boundary-layer Cartesian coordinates: streamwise direction, normal to surface, and normal to streamwise direction, respectively
Γ = intermittency function, $\frac{1}{2} - \frac{1}{2}$ erf $[(y/\delta - 0.8)/0.14(2)^{1/2}]$
γ = ratio of specific heats
δ = boundary-layer thickness, generally evaluated at y where $\bar{u} = 0.995u_e$
δ^* = displacement thickness, $\int_0^\delta \left(1 - \frac{\bar{\rho}\bar{u}}{\rho_e u_e}\right) dy$
δ_i^* = incompressible displacement thickness, $\int_0^\delta \left(1 - \frac{\bar{u}}{u_e}\right) dy$
ϵ = eddy viscosity, $-\langle(\rho v)'u'\rangle/(\partial\bar{u}/\partial y)$
ζ = ratio of local total enthalpy to external total enthalpy, $\bar{H}/H_e$
$\eta(x,y)$ = $u_e r^j \int_0^y \bar{\rho}\, \frac{dy}{\mu_s(2\xi)^{\bar{n}}}$
θ = momentum thickness, $\int_0^\delta \left(1 - \frac{\bar{u}}{u_e}\right)\frac{\bar{\rho}}{\rho_e}\frac{\bar{u}}{u_e}\, dy$
$\bar{\theta}$ = normalized total temperature profile, $\frac{\bar{H} - H_w}{H_e - H_w}$
θ_i = incompressible momentum thickness, $\int_0^\delta \left(1 - \frac{\bar{u}}{u_e}\right)\frac{\bar{u}}{u_e}\, dy$
μ = molecular viscosity
$\xi(x)$ = $\int_0^x \left[r^{2j}\frac{(\rho\mu u)_e}{\mu_s^2}\right] dx$
ρ = mass density
τ = shear stress

Subscripts

aw = adiabatic wall
e = flow conditions external to boundary layer
f = far wall region
M = evaluated at point where $M/M_e = 0.995$
n = near wall region
s = total or stagnation
w = wall conditions

Symbols

$(^-),\langle\ \rangle$ = time mean value
$(\ )'$ = fluctuating quantity

Introduction

SEVERAL numerical methods developed primarily for the calculation of incompressible turbulent flows have been extended recently to the calculation of compressible turbulent boundary layers.[1-4] The numerical procedures used in these methods differ considerably; however, the formulation of terms for the turbulent flux of momentum and heat is nearly the same in three of the methods.[1-3] An eddy viscosity concept is used in these methods with Prandtl's mixing length relation utilized for the wall region. This relation is modified in the near wall region by a suitable damping function such as that of Van Driest.[5] In the outer region the eddy viscosity relation of Clauser[6] is used in the first two methods[1,2] with the incompressible displacement thickness retained as the length scale.

Received June 11, 1969; presented as Paper 69-684 at the AIAA Fluid and Plasma Dynamics Conference, San Francisco, Calif., June 16–18, 1969; revision received January 21, 1970.

* Head, Flow Analysis Section, Aero-Physics Division.
† Head, Gas Dynamics Section, Aero-Physics Division. Associate Fellow AIAA.

In the method of Patanker and Spalding,[3] the mixing length is taken as a universal function of the distance from the wall and the boundary-layer thickness. This function is similar to that proposed by Maise and McDonald[7] as invariant for adiabatic boundary layers up to Mach 5. In the eddy viscosity methods[1-3] the turbulent flux of heat is computed from the differential equation for the total enthalpy with the turbulent Prandtl number generally taken as unity.

In the method of Bradshaw and Ferriss,[4] the eddy viscosity concept is abandoned in favor of a differential equation for the turbulent shear that is based on the kinetic energy equation for the turbulent velocity fluctuations. In this method, Crocco's linear relation between total enthalpy and velocity provided the solution to the mean energy equation.

It is perhaps remarkable that all four of these methods[1-4] have been uniformly successful in the prediction of incompressible boundary layers as shown at the recent Stanford conference.[8] Application of the methods to compressible flows has so far been limited mainly to adiabatic boundary layers where the predictions of skin friction and velocity profiles up to about Mach 5 have been satisfactory. Adiabatic skin-friction predictions from the method of Patanker and Spalding were in good agreement with the correlation of Spalding-Chi[9] up to Mach 10.

Calculation of a nonzero pressure gradient case was reported by Herring and Mellor[2] who obtained good predictions of displacement and momentum thicknesses on a waisted body.[10] The predictions of skin friction and velocity profiles were not as good, possibly because of effects in the experiment due to lateral curvature and centrifugal accelerations that are not accounted for in the theory.

The successful application to adiabatic flows of the eddy viscosity methods[1-3] indicates that simple modifications to the eddy viscosity models and also to the turbulent Prandtl number might provide useful predictions for nonequilibrium and high-speed flows with large heat transfer. The main purpose of the present paper is to determine what modifications, if any, to these models and to the value or distribution of the turbulent Prandtl number, will provide acceptable predictions of nonequilibrium and hypersonic boundary layers with cold walls. Predictions for velocity, temperature, and Mach number profiles as well as skin friction and heat transfer are compared with experimental data. Test cases include the effects of wall blowing, downstream recovery from wall blowing, and tunnel wall boundary layers. The tunnel wall boundary layers are of interest because of possible nonequilibrium effects that may account for differences between nozzle wall and flat-plate boundary layers (see Refs. 11, 12, and paper 11 of Ref. 13). Additional results from the present method are reported in paper 18 of Ref. 14. The method has been extended to quasi-three-dimensional boundary layers in paper 19 of Ref. 14.

Synopsis of Method

Numerical solutions to the differential equations for mean momentum, total enthalpy, and continuity are obtained by a finite-difference procedure similar to that of Ref. 15. Models of the terms for the turbulent flux of momentum and heat of Refs. 3 and 7 are modified to account for nonequilibrium flows and the effects of fluctuating density which may become important at hypersonic speeds.

Basic Equations

The conservation equations are written in essentially the same form as given in Ref. 2, except that the eddy viscosity and turbulent Prandtl number expressions are generalized to include the fluctuating density (see Nomenclature).

Continuity equation

$$(\partial/\partial x)(r^j\bar{\rho}\bar{u}) + (\partial/\partial y)(r^j\bar{\rho}\bar{v}) = 0 \tag{1}$$

where $j = 1$ for axisymmetric flow and $j = 0$ for two-dimensional flow.

Streamwise momentum equation

$$\bar{\rho}\bar{u}\frac{\partial\bar{u}}{\partial x} + \bar{\rho}\bar{v}\frac{\partial\bar{u}}{\partial y} = -\frac{dp_e}{dx} + \frac{\partial}{\partial y}\left[\mu\left(1 + \frac{\epsilon}{\mu}\frac{\partial\bar{u}}{\partial y}\right)\right] \tag{2}$$

Total enthalpy equation

$$\bar{\rho}\bar{u}\frac{\partial\bar{H}}{\partial x} + \bar{\rho}\bar{v}\frac{\partial\bar{H}}{\partial y} = \frac{\partial}{\partial y}\left\{\frac{\mu}{Pr}\left[\left(1 + \frac{\epsilon}{\mu}\frac{Pr}{Pr_T}\right)\frac{\partial\bar{H}}{\partial y} + (Pr - 1)\frac{\partial}{\partial y}\frac{\bar{u}^2}{2}\right]\right\} \tag{3}$$

To apply these equations to the calculation of turbulent boundary layers, initial profiles of $\bar{u}$ and $\bar{H}$ are required together with the usual boundary conditions at the wall and for $y \to \infty$. In the calculations, $y \to \infty$ is replaced by finite values of y where $\bar{u}/u_e$ and $\bar{H}/H_e \to 0.9999$.

For convenience in discussion, Eqs. (2) and (3) may be written in terms of the velocity profile F and the normalized total enthalpy profile $\bar{\theta}$,

$$\bar{\rho}\bar{u}\frac{\partial F}{\partial x} + \bar{\rho}\bar{v}\frac{\partial F}{\partial y} = -\rho_e u_e\left(1 - \frac{\bar{\rho}}{\rho_e}F^2\right)\frac{dp_e/dx}{\rho_e u_e^2} + \frac{\partial}{\partial y}\left[\mu\left(1 + \frac{\epsilon}{\mu}\right)\frac{\partial F}{\partial y}\right] \tag{2a}$$

$$\bar{\rho}\bar{u}\frac{\partial\bar{\theta}}{\partial x} + \bar{\rho}\bar{v}\frac{\partial\bar{\theta}}{\partial y} = -\bar{\rho}\bar{u}(1 - \bar{\theta})\frac{dH_w/dx}{H_e - H_w} + \frac{\partial}{\partial y}\left[\frac{\mu}{Pr}\left(1 + \frac{\epsilon}{\mu}\frac{Pr}{Pr_T}\right)\frac{\partial\bar{\theta}}{\partial y}\right] + \frac{\partial}{\partial y}\left(\frac{\mu}{Pr}\frac{Pr - 1}{H_e - H_w}\frac{\partial}{\partial y}\frac{\bar{u}^2}{2}\right) \tag{3a}$$

Since F and $\bar{\theta}$ must satisfy the same boundary conditions, Eqs. (2a) and (3a) give the familiar result that $\bar{\theta} = F$ when p_e and H_w ($= C_pT_w$) are constant and $Pr = Pr_T = 1.0$. For the more general situation, a negative wall temperature gradient would have much the same effect on $\bar{\theta}$ as a negative pressure gradient would have on F. Also, because usually $\epsilon/\mu \gg 1.0$ (except very near the wall), an increase in Pr_T reduces the turbulent flux of $\bar{\theta}$ in precisely the same way as a corresponding decrease in ϵ would reduce the turbulent flux of F or momentum.

Eddy viscosity expression

The expanded Reynolds stress term is

$$\langle(\rho v)'u'\rangle = \bar{\rho}\langle v'u'\rangle + \bar{v}\langle\rho'u'\rangle + \langle\rho'v'u'\rangle \tag{4}$$

where the last two terms are generally neglected. However, for hypersonic flow conditions where the boundary-layer thickness may increase rapidly and the density gradients are large, these terms may become significant. In fact, an order of magnitude analysis shows if $\bar{v}$ and ρ' are considered for these conditions to be the order of $(\delta)^{1/2}$ and 1, respectively, that the last two terms of Eq. (4) are the only additional fluctuating terms from the complete momentum equation that should be retained. [In this analysis it is assumed that y is the order of δ, u' and v' are the order of $(\delta)^{1/2}$, and all μ' terms are neglected.] To investigate the relative magnitudes of the terms in Eq. (4), they are modeled as follows:

$$\epsilon \equiv -\frac{\langle(\rho v)'u'\rangle}{\partial\bar{u}/\partial y} = \Gamma\left(\bar{\rho}l^2\left|\frac{\partial\bar{u}}{\partial y}\right| - \bar{v}l^2\frac{\partial\bar{\rho}}{\partial y} - l^3\left|\frac{\partial\bar{u}}{\partial y}\right|\frac{\partial\bar{\rho}}{\partial y}\right) \tag{5}$$

where the mixing length l is assumed the same in all terms and is expressed as

$$l/\delta = [1 - \exp(-y/A)]f(x,y/\delta) \tag{6}$$

The justification for assuming that this simple l/δ function applies to all three terms of Eq. (5) is based on results of Ref. 16. The quantity $A = A^*\mu/\rho(\tau/\rho)^{1/2}$ reduces to the form

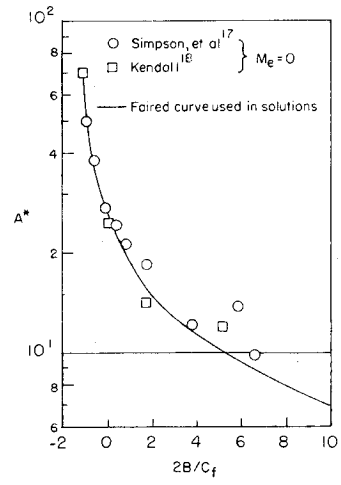

Fig. 1 Variation of "damping constant" with blowing parameter.

originally proposed by Van Driest[5] if $A^* = 26$. The shear and gas properties which appear in this expression for A are generally evaluated herein at the wall. For applications to wall blowing cases, A^* is assumed to be a function of the blowing parameter $2B/C_f$ as obtained from incompressible data.[17,18] These values of A^* are shown in Fig. 1 and were taken as the values of $\rho y u_{\tau_w}/\mu$ where the data near the wall first deviate from a straight line fairing in semilog plots of u/u_{τ_w} against $\rho y u_{\tau_w}/\mu$. It has been shown[19] that the scaling factor $2B/C_f$ includes any Mach number and wall temperature effects within the range and scatter of the presently available data. Hence, the solid line fairing in Fig. 1 was used in the present calculations. Predictions obtained with this fairing and with $A^* = 26$ (constant as in Refs. 1 and 3) will be compared with experimental data from a test case with blowing.

Maise and McDonald[7] have shown that mixing length values for incompressible equilibrium flows can be used for compressible equilibrium flows with adiabatic walls. The present mixing length function $f(x,y/\delta)$ is based on the results of Ref. 7 but modified herein to account for nonequilibrium effects. That is, for the far wall region ($y/\delta \geq 0.3$), the assumption is made that $f_f = (l/\delta)_f$ is a function of $H_i{}^*$, rather than $f_f \approx 0.09$ as in Ref. 7. The function $f_f(H_i{}^*)$ is based on incompressible data shown in Fig. 2. The data from Refs. 20–25 represent the average values of l/δ in the region $0.3 < y/\delta < 0.6$. The data of Simpson were evaluated at $y/\delta = 0.5$ (Ref. 26) which may account for the somewhat larger values than the average shown for all other data. Since the data are not conclusive, three arbitrary fairings were used in the present calculations. Some of the apparent scatter in the data of Fig. 2 may be caused by different upstream histories in the various flows. That is, $(l/\delta)_f$ is probably not a function of $H_i{}^*$ only. The variations used herein merely represent a convenient artifice to partially account for nonequilibrium effects.

The present mixing length function for the inner wall region ($y/\delta \leq 0.1$) is Prandtl's wall slope; $f_n = 0.4\, y/\delta$. A straight line segment is then used to join the inner and far wall regions between $y/\delta = 0.1$ and $y/\delta = 0.3$.

Turbulent Prandtl numbers

The turbulent Prandtl number used in Eq. (3) is based on the total enthalpy gradient and will be referred to as the total Prandtl number Pr_T. Since the conventional turbulent Prandtl number, herein designated as Pr_t, is defined in terms of the static enthalpy gradient, it is useful to review the relation between the two Prandtl numbers.

If $\bar{v}/\bar{u} \ll 1$, $\langle u'^2 + v'^2 + w'^2\rangle/\bar{u}^2 \ll 1$, and third-order correlations are neglected, it can be shown from the definitions of the instantaneous total enthalpy and the turbulent Prandtl numbers Pr_T and Pr_t (see Nomenclature) that

$$Pr_T = Pr_t\left[1 + \frac{u_e^2}{2H_e}(Pr_t - 1)\frac{\partial F^2}{\partial y}\Big/\left(1 - \frac{T_w}{T_{s,e}}\right)\frac{\partial \bar{\theta}}{\partial y}\right]^{-1} \quad (7)$$

Experimental data[11,12] show that in the outer part of a turbulent boundary layer the relation between $\bar{\theta}$ and F can be approximated as

$$\bar{\theta} = F^n \quad (8)$$

where $n \approx 1.0$ for flat-plate type of flows and $n \approx 2.0$ for nozzle wall flows. Differentiation of Eq. (8) and substitution into Eq. (7) then yields

$$Pr_T = Pr_t\left[1 + \frac{\gamma - 1}{n} M_e^2 (Pr_t - 1)\bar{\theta}^{(2-n)/n}\Big/\left(1 + \frac{\gamma - 1}{2} M_e^2\right)\left(1 - \frac{T_w}{T_{s,e}}\right)\right]^{-1} \quad (9)$$

where C_p and γ were assumed constant. Pr_T from Eq. (9) is plotted against Pr_t in Fig. 3 for several values of $T_w/T_{s,e}$, $\bar{\theta}$, M_e, and $n = 1$ and 2. The trends shown on this figure should be regarded as rough guides for the levels of total Prandtl number Pr_T based on knowledge of trends in static Prandtl number Pr_t.

Although data for Pr_t are still somewhat inconclusive, most of the incompressible data for the far wall region of pipe flows[27] and boundary layers[28,29] indicate $Pr_t \approx 0.5$–0.9. The same data generally indicate that Pr_t increases to a peak of about 0.8 to 1.0 as the wall is approached and then drops off again near the wall to 0.5 to 0.7. Flat-plate data at Mach number 5 (Ref. 30) with values of $T_w/T_{s,e}$ from 0.44 to 0.91 indicate $Pr_t \approx 1.0$ in the outer part of the boundary layer with Pr_t again decreasing to 0.7 to 0.9 near the wall. On the other hand, values quoted by Rotta[11] indicate that Pr_t may increase to 2 or more as the wall is approached.

In the light of these results, the best that can be said regarding the use of Fig. 3 as a guide is that there appears to be some justification for the use of larger values of Pr_T near the wall for nozzle wall flows than for flat-plate flows (compare Figs.

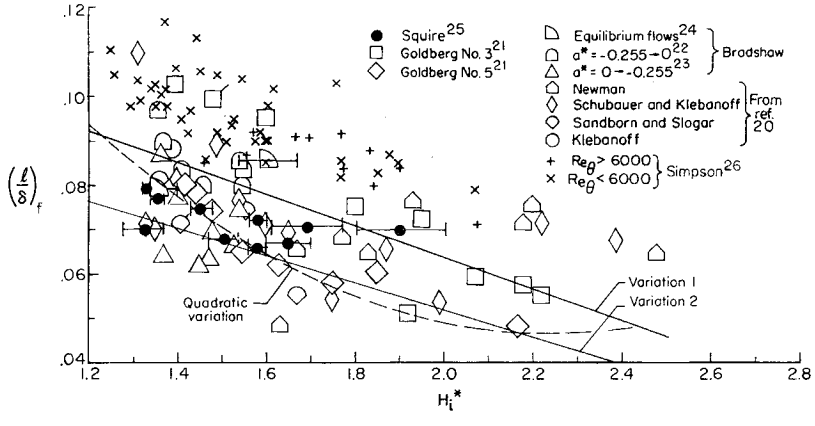

Fig. 2 Variation of mixing length in outer region of boundary layer with incompressible form factor.

3a and 3b). The implication of this statement is that Pr_T depends on the upstream history of the flow, and in particular, the quadratic variation between $\bar{\theta}$ and F as observed for tunnel wall boundary layers could be accounted for if Pr_T exceeds unity as will be shown later. In the absence of better data for turbulent Prandtl numbers, the final choice has to depend on the agreement between the calculated and experimental wall fluxes and profiles.

Numerical Procedure

For the sake of brevity the computational equations will not be included in this paper. These equations are derived in the usual manner by transforming Eqs. (1–3) to the variables η and ξ (see Nomenclature). The main purpose of this transformation is to minimize the boundary-layer growth in the transformed plane. That is, the number of $\Delta\eta$ steps across the boundary layer can be kept nearly constant by adjusting the values of $\bar{n}$. For laminar flows $\bar{n} = \frac{1}{2}$ but for turbulent flows its value is usually in the range $0.8 < \bar{n} < 1$.

The transformed equations are integrated all the way to the wall by an implicit finite-difference procedure which, in most respects, is identical to that of Ref. 15. The derivatives in the ξ direction are replaced by two-point central difference quotients, and three-point difference quotients are used in the η direction. The resulting algebraic equations for continuity, momentum, and energy are linearized individually but solved simultaneously by a "round robin" iteration procedure. To increase the accuracy and efficiency, a variable grid size in the η direction is used.

Results and Discussion of Test Cases

For brevity, the results of only four test cases will be presented herein. These four cases cover a wide range of flow conditions and include illustrations of nonequilibrium effects due to upstream conditions of blowing, wall temperature gradients, and favorable pressure gradients. Predictions of skin-friction and velocity profiles for the equilibrium, adiabatic flow of Moore and Harkness[31] were satisfactory. Acceptable results for severe adverse pressure gradients have also been obtained (paper 18, Ref. 14).

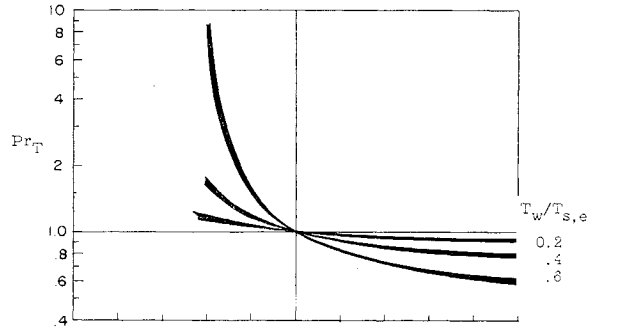

a) $n = 2$ (simulates nozzle wall boundary layers); curves apply for all values of $\bar{\theta}$

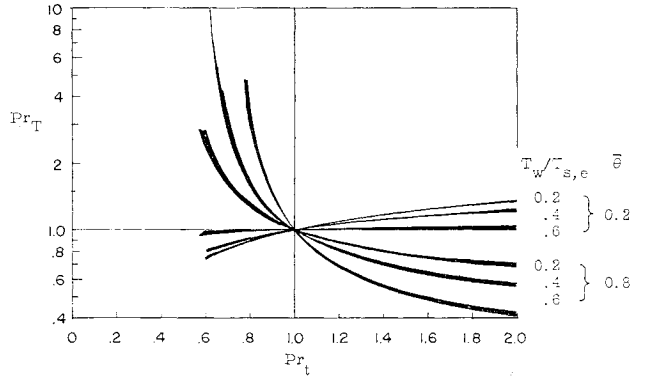

b) $n = 1$ (simulates flat plate boundary layers); curves for $\bar{\theta} = 0.5$ would be identical to those of Fig. 3a

Fig. 3 Approximate relations from Eq. (9) between turbulent Prandtl numbers based on total (Pr_T) and static (Pr_t) enthalpy gradients. The shaded bands are for the Mach number range, $8 \leq M_e \leq 18$.

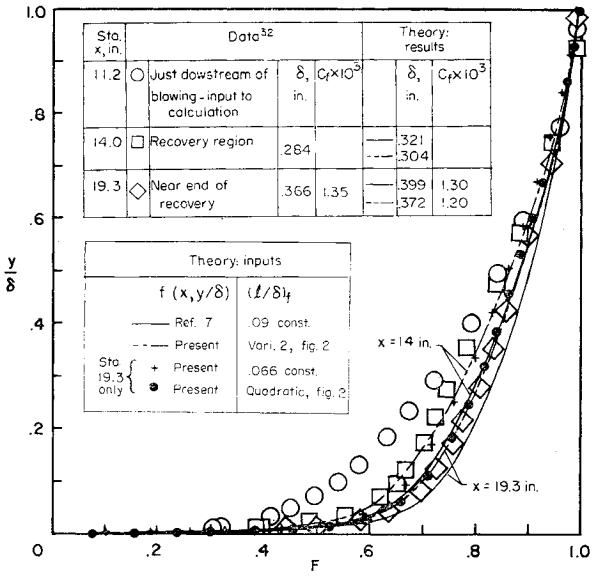

Fig. 4 Experimental[32] and theoretical velocity profiles for recovery from blowing.

The general philosophy adopted throughout this investigation has been to utilize the "numerical experiment" approach wherein the uncertain aspects of the proposed modifications to the models for the turbulent flux terms were introduced and/or varied one at a time. To determine the validity of the modifications, calculations are also obtained with the original models of Refs. 3 and 7.

Recovery from Wall Blowing

The investigation of Peterson et al.[32] was used as a test case for nonequilibrium flow. These data were obtained at Mach 3 for adiabatic wall conditions on a flat plate. The plate was 24 in. long with a flush mounted porous section that extended from $x = 3$ to 11 in. from the leading edge. Air was injected into the boundary layer through the porous section. Profile measurements were obtained just downstream of the porous section and at two stations further downstream where the profile was adjusting to correspond to the impermeable wall boundary condition.

The data as obtained from Fig. 15(a) of Ref. 32 are shown on Fig. 4. The calculations were initiated at the 11.2-in. station just downstream of the porous section and were continued to the 19.3-in. station where recovery from the blown profile was almost complete. All inputs and boundary conditions were held fixed except the f and $(l/\delta)_f$ functions which were varied as indicated. The $(l/\delta)_f$ functions are given in Fig. 2. The H_i* input value was 1.55. The results indicate, as might be expected, that a decrease in the mixing length in the outer region (corresponding to a decrease in the eddy viscosity) causes a less full velocity profile and a value of δ in closer agreement with experiment. The use of variation 1 (Fig. 2) gave results almost identical to those obtained with the f function from Ref. 7. The use of variation 2 appears to account satisfactorily for nonequilibrium or upstream history effects and gives better results than the unmodified function of Ref. 7. In an attempt to determine whether the level of $(l/\delta)_f$ or its variation with H_i* were responsible for these results, two additional solutions were obtained with the present f function. The velocity profiles from these solutions are compared with the data at the 19.3-in. station in Fig. 4. Comparison of these results with the other predictions and

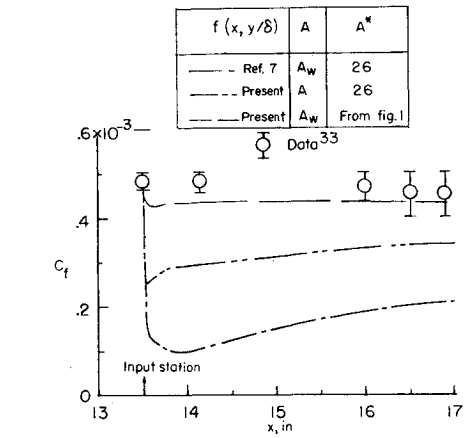

a) Skin-friction results

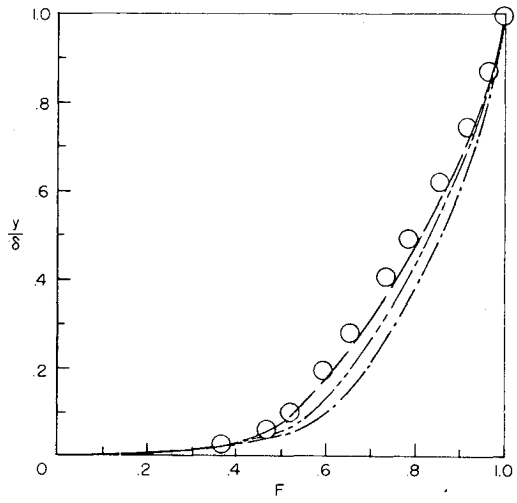

b) Velocity profiles at 16-in. station (see Fig. 5a for key)

Fig. 5 Test case with blowing at wall, $M_e = 3.54$, $B = 1.22 \times 10^{-3}$.

the data at the 19.3-in. station shows that reducing the level of $(l/\delta)_f$ from 0.09 (Ref. 7) to 0.066, corresponding to the initial value as required in the use of variation 2, underpredicts the values of F. The quadratic variation, which increases from about 0.066 to 0.085 over the length of the test flow, appears to be in the best agreement with the data. It can be concluded that for this particular flow, the use of an $(l/\delta)_f$ function similar to either variation 2 or the quadratic variation gives the best agreement with data near the end of the relaxation region.

Wall Blowing

Another test case, useful for studying the response of the solutions to changes in boundary conditions, is that of blowing at the wall. The only modification necessary in the present method to compute a wall blowing case is to input the local values of v_w as a boundary condition. However, as noted previously, modifications to the eddy viscosity function may be necessary due to the possible effect of the wall blowing on the structure of the turbulence in the near wall region.

The test case chosen was that of Jeromin[33] where data were obtained at several x stations on a porous plate. Measured values of δ, H^*, and Re_θ were given at several x stations. The runs used were numbers 3.5-1.2-3.1 to 3.5-1.2-3.8 ($M_e = 3.54$) of Ref. 33.

The calculated values of C_f are compared with the data on Fig. 5a. The measured value of C_f without blowing was 1.27×10^{-3}. Again, several solutions have been obtained to investigate the effect of various changes in the mixing length function as indicated on the figure. It can be seen that the agreement with data is poor unless A^* is taken from Fig. 1, although if A is evaluated at the local y (as recommended by Patanker and Spalding[8]), the agreement is much improved even with $A^* = 26$. The unmodified f function of Ref. 7 and the use of $A^* = 26$ results in unsatisfactory predictions for C_f.

The predictions for δ, Re_θ, and H^* (not shown herein) were in good agreement with the data and were generally improved by the use of the present f function and A^* from Fig. 1.

The velocity profiles are compared on Fig. 6b, and the best agreement is again obtained with the present f function and A^* from Fig. 1. Hence, the indications from this one test case are that the modified mixing length function can be extended to boundary layers with mass transfer by adjusting the damping factor to account for the change in mean velocity profiles near the wall.

Nozzle Wall Boundary Layers

Preliminary results of the present investigation were given in paper 11 of Ref. 13. Calculations for a Mach 8 nozzle wall boundary layer were presented and the results indicated that a better assessment of the prediction method could be obtained from a test case where both the initial upstream profiles and the final profiles at a downstream station are available from experimental data. Such a test case is considered first.

Mach number 11 conical nozzle

Pitot pressure and stagnation temperature measurements[34] were made across the boundary layer on the wall of a 7.5° (total angle) conical nozzle in a hypersonic gun tunnel facility. Data were obtained at two stations 8 in. apart in the flow direction. Heat-transfer measurements were made with thin film gages and skin friction was obtained from wall slopes of velocity profiles and from applications of the Baronti-Libby transformation.[35]

The boundary conditions and the initial profiles for velocity and total temperature used in the solutions were taken from the experimental conditions. Other conditions used were: $T_w/T_{s,e} = 0.28$, $p_s = 4400$ psia, and $T_{s,e} = 1020°$K.

The effects of the different $(l/\delta)_f$ variations, the level and variation of turbulent Prandtl numbers, and the density fluctuation terms in the eddy viscosity expression [Eqs. (4) and (5)] were investigated in five solutions. Results from these five solutions are compared with data in Fig. 6 where $\bar{\theta}$ is plotted against F. For all these solutions, the present mixing length function $f(x,y/\delta)$ was used because the results from the previous test cases indicated that the present function gave better results than the unmodified function from Ref. 7. The turbulent Prandtl numbers used in solutions 4

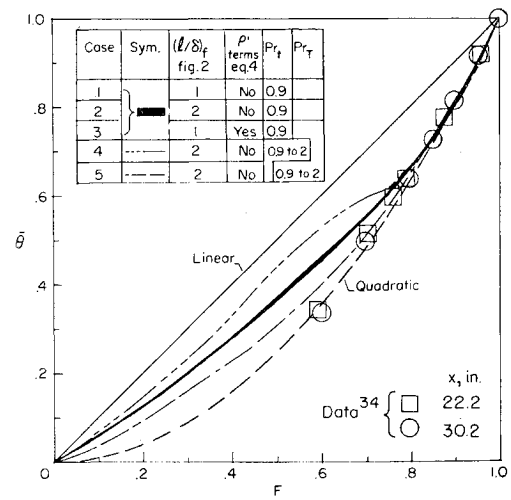

Fig. 6 Variation of normalized total temperature parameter with velocity ratio.

and 5 were varied across the boundary layer from 0.9 at the wall to 2.0 in the outer part of the boundary layer for $y/\delta > 0.05$.

Comparisons, not shown herein, of computed profiles for F, ζ, and M/M_e with experimental data indicated that for this high Reynolds number case the profiles are insensitive to changes in turbulent Prandtl number and eddy viscosity, and good agreement with data was obtained. On the other hand, the variation of $\bar{\theta}$ with F, for $F < 0.8$ (Fig. 6) is affected considerably by a change in turbulent Prandtl number, but is insensitive to any of the other changes made. The only way the observed quadratic type $\bar{\theta}$-F relation could be obtained in the inner region of the boundary layer ($F < 0.8$) was to use values for Pr_T that are greater than unity. However, the $\bar{\theta}$-F quadratic relation was always obtained in the outer part of the boundary layer where $F > 0.8$. To determine the effect of Reynolds number on the predictions, results from another test case with a smaller Reynolds number are compared with experimental data.

Mach number 18 contoured nozzle

Pitot pressure and stagnation temperature surveys of the boundary layer on the wall of a Mach 18 nozzle have been made by F. L. Clark and W. D. Harvey of the NASA Langley Research Center. The test gas was nitrogen with less than 5 ppm of oxygen. The facility and its operation were described and some of the preliminary boundary-layer data (from Pitot pressure measurements only) were reported by Clark et al.[36] The present data are still considered preliminary due to the large corrections that had to be applied to the stagnation temperature measurements for radiation and conduction losses. These corrections affect only the F and ζ profiles and the resulting maximum uncertainties in the ζ profile are estimated as ± 10 percent in the midregion of the boundary layer. Also the present Pitot pressure data have not been corrected for rarefaction effects. Application of such corrections could reduce the Pitot pressures and Mach numbers near the wall significants amounts. All data reduction and correction procedures used for these nozzle wall data will be available in a NASA publication by Harvey, Clark, and Beckwith.

The boundary conditions used in the calculation are shown in Fig. 7. The throat of the nozzle is at $x = 0$ and the station where the boundary-layer data were obtained is at $x = 82$ in. Since the upstream wall temperature in the nozzle was not measured, two different distributions designated $\zeta_{w,1}$ and $\zeta_{w,2}$ in Fig. 7 were used in the calculations in an attempt to evaluate the effects of the wall temperature history on the boundary layer at the data station. Stagnation conditions used in all calculations were $T_{s,e} = 3070°$R and $p_s = 7040$ psia.

Boundary-layer thicknesses and skin friction from seven solutions are compared with the data in Table 1 where the various inputs and boundary conditions used in the solutions

Table 1 Theoretical inputs and results for Mach 18 nozzle wall boundary layer

Case	Line Symbol fig. 8 and 9	Inputs: ζ_w fig. 7	$f(x,\frac{y}{\delta})$ fig. 2	Pr_t	Pr_T	Γ	p' terms eq. (5)	Outputs at x = 82 in.: $\frac{2St}{C_f}$	$C_f \times 10^4$	δ in.	δ_M in.	$\bar{\theta} \times 10^2$ in.
1	—●—●—	1	1	0.9	---	No	No	1.05	6.48	3.61	4.20	4.13
2	- - - —	1	1 and 2	0.9	---	No	No	1.10	5.32	3.70	4.07	4.30
3	—— —	2	2	0.9	---	No	No	1.09	5.13	4.60	4.97	8.90
4	- - —	2	2	---	see sketch[a]	No	No	0.85	5.22	4.44	5.00	7.97
5	x	2	2	---	see sketch[a]	No	No	0.92	5.10	4.48	4.98	8.37
6	+	2	2	---	same as 5	Yes	No	0.90	5.20	4.03	4.27	8.03
7	▮	2	2	---	see sketch[a]	Yes	Yes	0.90	3.30	3.75	3.88	7.72
Data	○								4.4 to 7.7		3.7	6.85

[a] Figure 7.

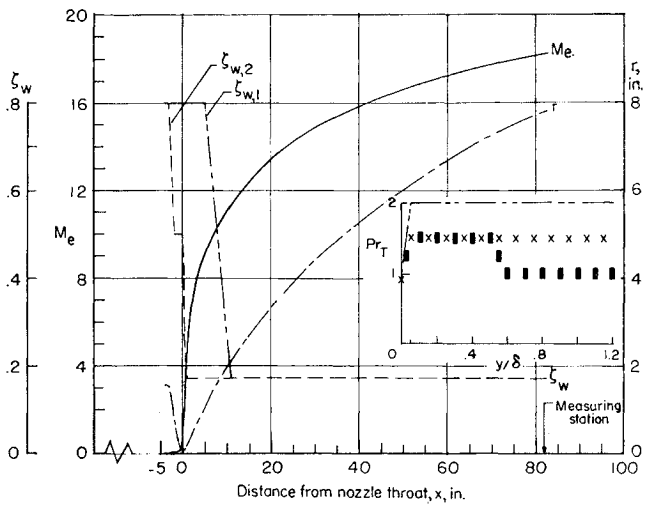

Fig. 7 Boundary conditions and inputs for Mach 18 nozzle wall boundary-layer calculations. Data were obtained for stagnation conditions of 2960° R $\leq T_{s,e} \leq$ 3240°R and 6000 psia $\leq p_{s,e} \leq$ 6560 psia.

are also given. Three different distributions for Pr_T were used in these solutions as shown in Fig. 7. All solutions were started 4 inches upstream of the throat ($x = -4$ in.) except solution 1 which was started at the throat ($x = 0$). The initial profiles for $\bar{\theta}$ and F were taken as $\frac{1}{7}$ power law profiles for all solutions. Also used throughout was $A = A_w$ with $A^* = 26$.

The computed values of skin friction from the different solutions varies over about the same range as the experimental values which were obtained from the Mach number gradient at the wall using the formula $C_f = \mu_w a_w (\partial M/\partial y)_w / \frac{1}{2}\gamma p_e M_e^2$. The Spalding-Chi correlation[9] predicts $C_f = 2.4 \times 10^{-4}$ which is 45–70% below the data.

Except for the values of θ from solutions 1 and 2, the predicted boundary-layer thicknesses shown in Table 1 are larger than the experimental results. It is also evident by comparison of the results from the first two solutions with solution 3 that the predicted values of δ and θ at $x = 82$ in. are affected considerably by the wall temperature distribution in the throat region from $x = -4$ to 10 in. The best agreement with the experimental values of θ and δ_M was from solution 7.

The profiles from the seven solutions at station 82 are compared with the corresponding experimental profiles on Figs. 8 and 9. The various inputs used in these solutions are given in Table 1. Consider first the effect of moving the initial station from the throat ($x = 0$) upstream into the approach section at $x = -4$ in. as shown by comparison of solutions 1 and 2. The values of F, ζ, and M were increased for $y/\delta < 0.5$, but the net effect on the $\bar{\theta}$-F profile was small.

Solution 3 was obtained with the more realistic wall temperature distribution $\zeta_{w,2}$ (see Fig. 7). Compared with solutions 1 and 2, the result was to reduce ζ significantly for $y/\delta > 0.3$, as might be expected, but to increase ζ for $y/\delta < 0.3$ (see Fig. 8). On the other hand, the values of F were hardly affected for $y/\delta > 0.5$, but were increased considerably for $y/\delta < 0.5$. The net effect on the $\bar{\theta}$-F variation (Fig. 9) was to improve the agreement with data over most of the boundary layer. The agreement with the Mach number profile is good for $y/\delta > 0.3$. These results illustrate the large persistent effects of the wall temperature history on hypersonic nozzle wall boundary layers. In particular, when the large negative gradient in wall temperature occurs further upstream, the local increases in $\bar{\theta}$ as required by Eq. (3a) do not persist to the downstream station. At the same time the increases in F caused by the large negative dp_e/dx values in the throat region are seen to persist for greater distances.

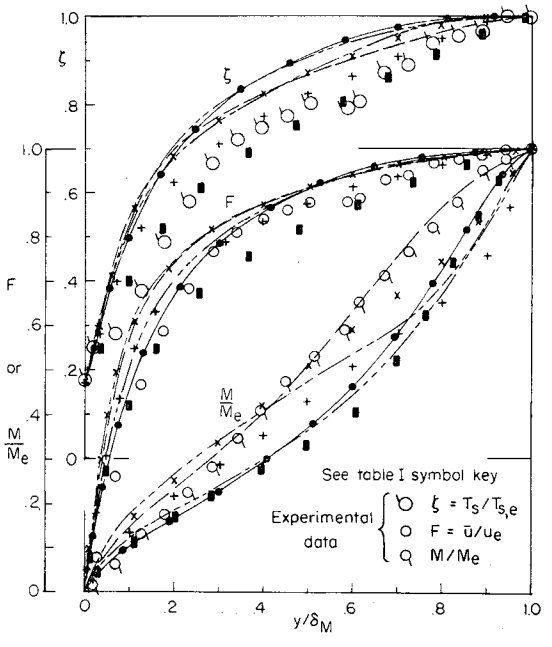

Fig. 8 Comparisons of calculated and experimental profiles in the turbulent boundary layer of a hypersonic nozzle at $x = 82$ in. where $M_e = 18.2$.

To determine the effect of adjustments to the turbulent Prandtl number from the nominal constant value of $Pr_t = 0.9$, solutions 4 and 5 were obtained. The discussion of Fig. 3 indicated that the total turbulent Prandtl number might assume values greater than unity. Also, the best agreement with data for the conical nozzle wall boundary layer just considered was obtained with $Pr_T = 2.0$ in the outer part of the boundary layer. Consequently, the same type of distributions for Pr_T (shown in Fig. 7) were used. Comparison of the results from solutions 4 and 5 with those from solution 3 show that the ζ and F profiles were not affected significantly, while the values of M were reduced for $y/\delta > 0.5$. The net result was the best agreement with the experimental $\bar{\theta}$-F variation as yet obtained (Fig. 9).

A study of these results for the Mach 18.2 nozzle flow and also the results for the conical nozzle of the previous section reveals a mechanism that may be responsible for the quadratic $\bar{\theta}$-F relation, provided that possible effects of nonuniform distributions in settling chamber temperature can be excluded (see paper 12 of Ref. 13). The mechanism may be described as follows. The large favorable pressure gradients in the approach and downstream of the throat increase the velocity [in accordance with Eq. (2a)] sufficiently to cause locally a quadratic $\bar{\theta}$-F variation in the outer part of the boundary layer. The increase in F also increases $\bar{\theta}$ since for large local Mach numbers and cold wall temperatures, $\bar{\theta}$ is nearly proportional to $\bar{u}^2$. When the Prandtl number is near unity, the $\bar{\theta}$-F relation therefore rapidly reverts to nearly a linear variation for $F < 0.7$. However, if the total turbulent Prandtl number is increased to 2.0, the effective turbulent transfer of total energy (or the eddy conductivity for $\bar{\theta}$) is reduced. $\bar{\theta}$ is then reduced [see Eq. (3a)] sufficiently so that the $\bar{\theta}$-F relation becomes quadratic over nearly the entire boundary layer and retains that shape far downstream in accordance with experimental data.

The values of turbulent Prandtl number also affect the Reynolds analogy factor $2St/C_f$ as shown in Table 1. The predicted values of Reynolds analogy factor with $Pr_t = 0.9$ are about 1.1 which is somewhat smaller than values obtained for flat plate flows as shown in Ref. 11. When values of $Pr_T > 1$ are used as inputs the Reynolds analogy factor decreases to about 0.9. These trends would be expected since $2St/C_f \propto (\partial\bar{\theta}/\partial F)_w$.

The agreement between solutions 4 and 5 with the Mach number profile data (Fig. 8) was not so good for $y/\delta > 0.5$, apparently due to a slight increase in ζ and reduction in F for the outer part of the profiles. These small changes were large enough to reduce the Mach number by 25% or more. This extreme sensitivity of the Mach number to small changes in velocity or enthalpy is caused primarily by the fact that $2\bar{H}/\bar{u}^2$ is nearly unity for hypersonic Mach numbers.

Results from two more solutions are shown on Figs. 8 and 9 to illustrate the effects of the intermittency function Γ, and of the ρ' terms. Referring first to the $\bar{\theta}$-F relation (Fig. 9) it is seen that these profiles for solutions 5–7 are nearly identical. Comparison with results for the other solutions shows that the $\bar{\theta}$-F profile for $F > 0.7$ responds mainly to the upstream history of pressure and wall temperature gradients. For $F < 0.7$, this profile approaches a quadratic variation only if $Pr_T \geq 1.5$ over at least the inner part of the boundary layer. These responses of the $\bar{\theta}$-F profile are again independent of the eddy viscosity which was reduced by a large amount when the Γ function and the ρ' terms were included as in solutions 6 and 7.

In contrast to the Mach 11 results, however, these changes in ϵ cause large changes in the F, ζ, and M/M_e profiles. This much greater response of these profile shapes to changes in ϵ for the Mach 18 flow as compared to the Mach 11 flow is apparently related to the different densities for the two test cases. That is, the smaller values of density for the Mach 18 flow (where ρ_e was about 0.05 of the value for the Mach 11 case) results in smaller values of ϵ [see Eq. (5)] which causes the F and ζ profiles to be less full. These types of profiles are evidently more sensitive to changes in ϵ than the more full profiles obtained in the higher density Mach 11 flow.

The sum of the ρ' terms (which for the solutions shown reduces ϵ for $y/\delta > 0.1$) from solution 7 at $x = 82$ in. were nearly as large as the usual Reynolds stress term. The sum of these terms was at most 0.3 of the Reynolds stress term for the Mach 11 case.

Concluding Remarks

The recovery of a turbulent boundary layer from the upstream effects of blowing was predicted satisfactorily for an adiabatic Mach 3 flow. This prediction was obtained by assuming the mixing length in the midregion of the boundary layer depends on both the boundary-layer thickness and the incompressible form factor rather than depending only on the boundary-layer thickness as in previous methods.

The effect of local blowing could be accounted for by the additional assumption that the wall damping factor of Van Driest is a function of the blowing rate.

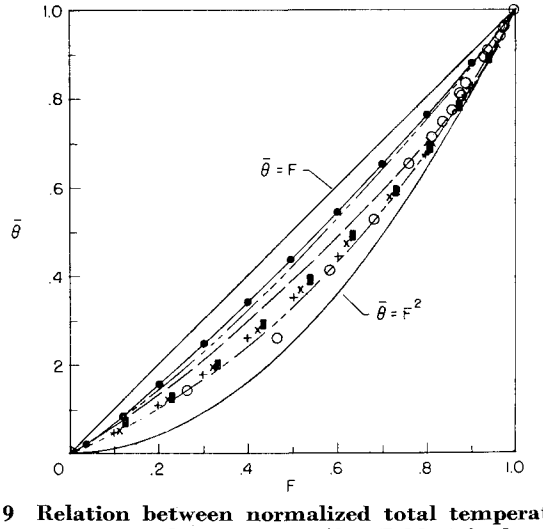

Fig. 9 Relation between normalized total temperature parameter and velocity ratio. (See Table I for key.)

The nozzle wall boundary layers showed large nonequilibrium effects, particularly apparent in the variation of the total enthalpy with velocity. The results of several solutions for the boundary layer on the walls of Mach 11 and 18 nozzles indicated that the observed quadratic behavior of the $\bar{\theta}$-F relation in the outer part of the boundary layer was caused by the upstream pressure and temperature gradients. However, the quadratic variation nearer the wall could not be obtained in the solutions without increasing the "total" turbulent Prandtl number Pr_T (based on the total enthalpy gradient) from near unity to 1.5 or more.

While the response of the $\bar{\theta}$-F relation to changes in Pr_T was essentially the same for both test cases, the velocity and total temperature profiles for the Mach 18 case were much more sensitive to changes in eddy viscosity than these profiles for the Mach 11 case. This different response for the two test cases was attributed to the smaller density for the Mach 18 case.

Solutions for the high Mach number nozzle flows have also shown that the fluctuating density terms in the eddy viscosity model may have to be considered for hypersonic turbulent boundary layers.

References

[1] Cebeci, T., Smith, A. M. O., and Mosinskis, G., "Recent Progress in the Calculation of Turbulent Boundary Layers," Douglas Paper 5531, May 1969, Douglas Aircraft Co., Long Beach, Calif.

[2] Herring, H. J. and Mellor, G. L., "A Method of Calculating Compressible Turbulent Boundary Layers," CR-1144, Sept. 1968, NASA.

[3] Patankar, S. V. and Spalding, D. B., *Heat and Mass Transfer in Boundary Layers*, Morgan and Grampian, London, 1967.

[4] Bradshaw, P. and Ferriss, D. H., "Calculation of Boundary-Layer Development Using the Turbulent Energy Equation. II—Compressible Flow on Adiabatic Walls," NPL Aero Report 1217, Nov. 24, 1966, National Physical Lab., Aerodynamics Div., Teddington, England.

[5] Van Driest, E. R., "On Turbulent Flow Near a Wall," *Journal of the Aeronautical Sciences*, Vol. 23, No. 11, Nov. 1956, pp. 1007–1011.

[6] Clauser, F. H., "The Turbulent Boundary Layer," *Advances in Applied Mechanics*, Vol. IV, Academic Press, New York, 1956, pp. 1–51.

[7] Maise, G. and McDonald, H., "Mixing Length and Kinematic Eddy Viscosity in a Compressible Boundary Layer," *AIAA Journal*, Vol. 6, No. 1, Jan. 1968, pp. 73–80.

[8] *1968 Conference on Turbulent Boundary Layer Prediction. Volume I: Prediction Methods and Physical Structure*, edited by S. J. Kline, D. J. Cockrell, and M. V. Morkovin, Stanford Univ., Dept. of Mechanical Engineering, Stanford, Calif.

[9] Spalding, D. B. and Chi, S. W., "The Drag of a Compressible Turbulent Boundary Layer on a Smooth Flat Plate With and Without Heat Transfer," *Journal of Fluid Mechanics*, Vol. 18, Pt. 1, Jan. 1964, pp. 117–143.

[10] Winter, K. G., Smith, K. G., and Gaudet, L., "Measurements of Turbulent Skin Friction at High Reynolds Numbers at Mach Number of 0.2 and 2.2," AGARDograph 97, *Recent Developments in Boundary Layer Research*, Pt. 1, May 1965, pp. 97–123.

[11] Rotta, J. C., "Heat-Transfer and Temperature Distribution in Turbulent Boundary Layers at Supersonic and Hypersonic Flow," AGARDograph 97, *Recent Developments in Boundary Layer Research*, Pt. I, May 1965, pp. 41–63.

[12] Bertram, M. H. and Neal, L., Jr., "Recent Experiments in Hypersonic Turbulent Boundary Layers," paper presented at the AGARD Specialists Meeting on Recent Developments in Boundary-Layer Research, Naples, Italy, May 10–14, 1965.

[13] Bertram, M. H., ed., *Compressible Turbulent Boundary Layers*, NASA SP-216, Dec. 10–11, 1968.

[14] *Analytic Methods in Aircraft Aerodynamics*, NASA SP-228, NASA Ames Research Center Symposium, Oct. 28–30, 1969.

[15] Beckwith, I. E. and Bushnell, D. M., "Detailed Description and Results of a Method for Computing Mean and Fluctuating Quantities in Turbulent Boundary Layers," TN D-4815, Oct. 1968, NASA.

[16] Harvey, W. D., Bushnell, D. M., and Beckwith, I. E., "Fluctuating Properties of Turbulent Boundary Layers for Mach Numbers up to 9," TN D-5496, Oct. 1969, NASA.

[17] Simpson, R. L., Kays, W. M., and Moffat, R. J., "The Turbulent Boundary Layer on a Porous Plate: An Experimental Study of the Fluid Dynamics With Injection and Suction," Rept. HMT-2, Dec. 1967, Stanford Univ., Dept. of Mechanical Engineering, Stanford, Calif.

[18] Kendall, R. M. et al., "Mass, Momentum, and Heat Transfer Within a Turbulent Boundary Layer with Foreign Gas Mass Transfer at the Surface. Part I—Constant Fluid Properties," Rept. 111, Feb. 1964, Vidya, Div. of Itek Corp., Palo Alto, Calif.

[19] Baronti, P., Fox, H., and Soll, D., "A Survey of the Compressible Turbulent Boundary Layer With Mass Transfer," *Astronautica Acta*, Vol. 13, Pergamon Press, New York, 1967, pp. 239–249.

[20] Escudier, M. P., "The Distribution of the Mixing Length in Turbulent Flows Near Walls," TWF/TN/1, March 1965, Mechanical Engineering Dept., Imperial College of Science and Technology, London, England.

[21] Goldberg, P., "Upstream History and Apparent Stress in Turbulent Boundary Layers," Rept. 85, May 1965, Gas Turbine Lab., Massachusetts Institute of Technology, Cambridge, Mass.

[22] Bradshaw, P. and Ferriss, D. H., "The Response of a Retarded Equilibrium Turbulent Boundary Layer to the Sudden Removal of Pressure Gradient," A.R.C. 26 758, May 1965, National Physical Lab., Aerodynamics Div., Teddington, England.

[23] Bradshaw, P., "The Response of a Constant-Pressure Turbulent Boundary Layer to the Sudden Application of an Adverse Pressure Gradient," A.R.C. 28 663, Jan. 1967, National Physical Lab., Aerodynamics Div., Teddington, England.

[24] Bradshaw, P., "The Turbulence Structure of Equilibrium Boundary Layers," A.R.C. 27 675, Jan. 1966, National Physical Lab., Aerodynamics Div., Teddington, England.

[25] Squire, L. C., private communication, March 1969, Cambridge Univ., Cambridge, England.

[26] Simpson, R. L., "Characteristics of Turbulent Boundary Layers at Low Reynolds Numbers With and Without Transpiration," April 1969, Thermal/Fluids Sciences, Institute of Technology, Southern Methodist Univ., Dallas, Texas.

[27] Kestin, J. and Richardson, P. D., "Heat Transfer Across Turbulent Incompressible Boundary Layers," *The Mechanics of Turbulence*, Gordon and Breach, New York, 1964, pp. 409–418.

[28] Johnson, D. S., "Turbulent Heat Transfer in a Boundary Layer With Discontinuous Wall Temperature," OSR TN 55-289, Aug. 1955, Dept. of Aeronautics, Johns Hopkins Univ., Baltimore, Md.

[29] Simpson, R. L., Whitten, D. G., and Moffat, R. J., "An Experimental Study of the Turbulent Prandtl Number of Air With Injection and Suction," *International Journal of Heat and Mass Transfer*, 1969.

[30] Rochelle, W. C., "Prandtl Number Distribution in a Turbulent Boundary Layer With Heat Transfer at Supersonic Speeds," DRL-508, Oct. 1963, Defense Research Lab., University of Texas, Austin, Texas.

[31] Moore, D. R. and Harkness, J., "Experimental Investigation of the Compressible Turbulent Boundary Layer at Very High Reynolds Numbers, $M = 2.8$," Rept. 0-71000/4R-9, Ling-Temco-Vought Research Center, Dallas, Texas.

[32] Peterson, J. B., Jr. et al., "Further Investigation of Effect of Air Injection Through Slots and Porous Surfaces on Flat-Plate Turbulent Skin Friction at Mach 3," TN D-3311, March 1966, NASA.

[33] Jeromin, L. O. F., "An Experimental Investigation of the Compressible Turbulent Boundary Layer with Air Injection," A.R.C. 28 549, Nov. 1966, Aeronautical Research Council, London, England.

[34] Perry, J. H. and East, R. A., "Experimental Measurements of Cold Wall Turbulent Hypersonic Boundary Layers," A.A.S.U. Report No. 275, Feb. 1968, AGARD Specialists' Meeting on Hypersonic Boundary Layers and Flow Fields, Royal Aeronautical Society of London.

[35] Baronti, P. O. and Libby, P. A., "Velocity Profiles in Turbulent Compressible Boundary Layers," *AIAA Journal*, Vol. 4, No. 2, Feb. 1966, pp. 193–202.

[36] Clark, F. L., Ellison, J. C., and Johnson, C. B., "Recent Work in Flow Evaluation and Techniques of Operations for the Langley Hypersonic Nitrogen Facility," presented at the Fifth Hypervelocity Techniques Symposium, Denver, Colo., March 28–30, 1967.